

pubs.acs.org/journal/estlcu Letter

Rapid Accumulation of Soil Inorganics on Plastics: Implications for Plastic Degradation and Contaminant Fate

Lauren N. Pincus,* Ajith Pattammattel, Denis Leshchev, Kewei Zhao, Eli Stavitski, Yong S. Chu, and Satish C. B. Myneni



Cite This: Environ. Sci. Technol. Lett. 2023, 10, 538-542



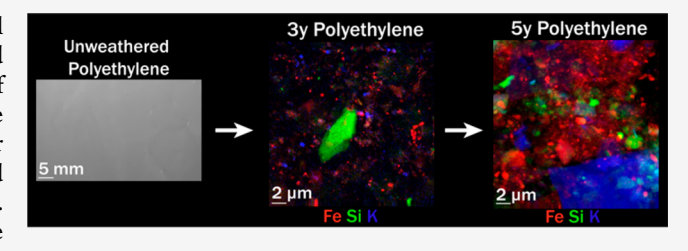
ACCESS I

Metrics & More

Article Recommendations

s Supporting Information

ABSTRACT: As plastics degrade in the environment, chemical oxidation of the plastic surface enables inorganics to adsorb and form inorganic coatings, likely through a combination of adsorption of minerals and in situ mineral formation. The presence of inorganic coatings on aged plastics has negative implications for plastics fate, hindering our ability to recycle weathered plastics and increasing the potential for plastics to adsorb contaminants. Inorganic coatings formed on terrestrially weathered polyethylene were characterized using synchrotron spectroscopy and micros-



copy techniques across spatial scales including optical microscopy, nano-X-ray-fluorescence mapping (nano-XRF), nano-X-ray absorption near edge structure (nano-XANES), and high-energy resolution fluorescence detected-XANES (HERFD-XANES). Results indicate a heterogeneous elemental distribution and speciation which includes inorganics common to soil terrestrial environments including iron oxides and oxyhydroxides, aluminosilicates, and carbonates.

KEYWORDS: plastics, spectroscopy, polymers, weathering, metal oxides

■ INTRODUCTION

Due to the exponential growth in the use of plastics and disposal of plastic waste since the 1960s, plastics have become one of the most widespread and persistent pollutants globally. Approximately 320 million tons of plastic are produced each year, and as much as 96% of these plastics are released into the environment or to landfills following their initial use. As plastics enter the environment, they are physically and chemically degraded into microplastics. Chemical weathering of the plastics includes oxidation of the plastic surface via UV photooxidation, photothermal degradation, and biodegradation. These chemical weathering processes can result in the development of oxygen-containing functional groups such as carbonyl, carboxyl, and hydroxyl groups, increasing the polarity and negative surface charge of plastics and potentially electrostatically attracting ions to form inorganic coatings.

The surface chemistry of microplastics is of particular concern as their small size increases their potential to be ingested by organisms, and their high surface area to volume ratio greatly increases their sorption capacity for pollutants, potentially resulting in biomagnification of toxins as plastics are ingested by organisms. Plastics are known as strong adsorbers of organic contaminants; however, they have also been found to contain up to thousands of ppb of toxic metals such as lead, mercury, and cadmium. Fouling of the plastic surface with inorganics likely controls sorption of toxic contaminants and negatively impacts the recyclability of these aged plastics.

Previous researchers such as Ashton et al.,⁴ Holmes et al.,⁶ and Holmes et al.⁷ noted the accumulation of hydrous metal oxides on plastics removed from marine and estuarine environments. Others such as Li et al.⁸ and Turner and Holmes⁹ have examined formation of inorganic coatings on plastics in laboratory conditions. However, accumulation of inorganics on terrestrially aged plastics has not yet been examined. It is expected that the type of inorganic coatings which form on degraded plastics, and the rate at which these reactions occur, will be strongly influenced by environmental conditions including terrestrial vs aqueous conditions.^{1,3} Therefore, this study aims to identify which inorganics adsorb to plastics weathered in a natural terrestrial environment using advanced spectroscopy techniques, as this important aspect of plastic fate has not yet been examined in detail.

METHODS AND MATERIALS

Experimental Setup. To naturally weather plastics, sheets of commercially available polyethylene (PE) (HDX clear low-density polyethylene plastic sheeting, 1 mm thick, Home Depot) were placed horizontally on both the soil surface and

Received: April 5, 2023 Revised: May 17, 2023 Accepted: May 19, 2023 Published: May 31, 2023





within a leaf mulch layer for two to five years in Princeton, NJ. In Princeton, NJ, the average temperature is 13 °C (range: -12 to 35 °C), the average relative humidity is 81% (range: 35%-100%), the average precipitable water is 2.3 cm (range: 0.2-6.5 cm), and the average global horizontal UV irradiance (280-400 nm) is 9.6 w/m^2 (range: $0-62 \text{ w/m}^2$) (all data from the National Solar Radiation Database, 2021). 10 PE was chosen due to its frequent societal use as greenhouse sheeting and plastic bags and its prevalence in the environment. The predominant soil types where the plastics were placed are WasA Watchung silt loam (~60%) and NehB (~25%) NehCb (~15%) Neshaminy silt loam. 11,12 The soil composition, analyzed via XRF, was ~9.7 wt % Al, ~22 wt % Si, ~0.78 wt % Mg, \sim 0.55 wt % P, \sim 0.11 wt % S, \sim 0.05 wt % Cl, \sim 1.4 wt % K, ~1.1 wt % Ca, ~0.16 wt % Mn, and ~5.6 wt % Fe. The elemental composition of the leaf mulch at this location is 800-2000 pm Al, 180-280 ppm Mg, 200-400 ppm K, 100-150 ppm Mn, and 800-1300 ppm Fe. The pH_w values of soil porewater and leaf leachates at this location were ~7.0-7.6 and ~4-4.5, respectively. 13 Upon conclusion of the experiment, the PE sheets were cleaned rigorously by hand with deionized (DI) water three times to remove any coatings not chemically adsorbed to the plastic surface. X-ray spectroscopy and optical and electron microscopies were used to characterize the inorganic distribution and speciation on the terrestrially weathered PE (2-, 3-, and 5-year samples). Samples were analyzed at National Synchrotron Light Source II (NSLS II) for nanoscale imaging using X-ray fluorescence (nano-XRF) (Figure 1), nanoscale iron (Fe) K-edge X-ray absorption near edge structure (nano-XANES)¹⁴ (Figure 2), and high-energy resolution fluorescence detected (HERFD)-XANES (Figure 2).

Instrumental Methods. Nano-XRF and Nano-XANES. Nano-XRF and nano-XANES experiments were conducted at the Hard X-ray nanoprobe (HXN) beamline at NSLS-II at Brookhaven National Laboratory. An X-ray beam of the size 30-50 nm was produced by a Fresnel zone plate with the outermost zone width of 30 nm. Details of the HXN instrumentation and data collection methods were published elsewhere. 14-16 Small fragments of terrestrially weathered PE were mounted on a small piece of Kapton tape for measurements. XRF maps were collected at 7.2 keV with aluminum, silicon, iron, manganese, calcium, phosphorus, sulfur, potassium, and chlorine analyzed. For XRF maps, 30 μ m \times 30 μ m scans were collected with a 0.01 s dwell time and 100 nm step, as well as 6 μ m × 6 μ m scans with a 0.04 s dwell time and 50 nm step. XRF data were fitted using PyXRF, ¹⁷ and image postprocessing was performed using FIJI. 1

For XRF fitting, an average XRF spectrum was produced by combining three fluorescence channels and all the points in the image grid. Elemental maps are generated by full spectrum deconvolution by fitting a model spectrum with the experimental data. A model spectrum was produced by PyXRF based on the peak positions and intensities. This spectrum was then updated with probable candidates from the elemental list and any escape or pile-up peaks accounted for. A nonlinear background was subtracted from the spectrum (SNIP, sensitive nonlinear iterative peak), and the Compton and elastic peaks were also modeled. The model spectrum was then fitted with the mean experimental spectrum using the non-negative least-squares (NNLS) method and visually inspected the truthfulness of the fit in addition to R-factor minimization. The optimized model parameters were then

applied to the spectrum at each pixel (pixel-wise fitting) to produce elemental maps. XRF quantitative analysis was performed using PyXRF by calibrating the counts with an XRF reference standard (MicroMatter) that was measured under the same experimental conditions. XRF correlation plots were created and analyzed using XMIDAS.¹⁹

For nano-XANES, Fe K-edge XANES stacks (69 energy points for 5-year PE, and 77 energy points for 3-year PE) were collected over the same 6 μ m × 6 μ m regions that had been analyzed via nano-XRF. Stacks were aligned and fitted via linear combination fitting (LCF) using a suite of iron mineral standards data collected at the Inner Shell Spectroscopy Beamline at NSLS II in transmission mode. Goodness of LCF fit was assessed via R-factor and by comparing the spectral features (e.g., pre-edge intensity and peak position) of regions of interest with mineral standards. Composite XANES LCF fit maps (speciation maps) were exported from XMIDAS 19 and compiled using FIJI.

HERFD-XANES. Iron K α X-ray emission-detected XANES data were collected at the Inner Shell Spectroscopy (ISS) beamline at NSLS-II.²⁰ Samples were loaded into sample holders and sealed in Kapton tape for analysis. The measurements were performed at room temperature. The beam was focused on the sample using a polycapillary optic down to a 100 μ m spot. High-energy resolution fluorescence detected (HERFD)-XANES were collected using a spherically curved Ge-440 crystal (radius of curvature 1 m) placed on a Rowland circle in Johann geometry. The spectrometer was set to the maximum of the $K\alpha$ emission. The emission was collected using a Pilatus detector. The absorption of the emitted X-rays in air was reduced by placing a helium enclosure between the sample, the crystal, and the detector. The data were collected using a continuous scanning approach with the duration of each HERFD scan set to 90 s. Each scan was taken at a fresh spot on the sample. Prior to data collection, each sample was tested for radiation-induced damage by performing repetitive rapid 10 s standard XANES scans for the duration of a single HERFD scan. In case samples exhibited changes in the XANES region within the series, the beam was attenuated until such changes were negligible compared to the noise in the data. Data were processed using Larch.²¹ Spectra were averaged, background-subtracted, normalized, and flattened. Data were analyzed via LCF within Larch²¹ using a suite of iron mineral standards also analyzed via Fe K α HERFD. The goodness of LCF fit was assessed via R-factor and by comparing spectral features (e.g., pre-edge intensity and peak position) of the samples with mineral standards.

■ RESULTS AND DISCUSSION

After terrestrial weathering, the plastics were observed to visibly degrade over time, becoming more fragile and prone to fragmentation into microplastics (Figure 1A, B). Development of oxygen-containing functional groups such as hydroxyl (3580–3100 cm⁻¹), ketone (1720 cm⁻¹), ester (~1740 and 1110–1050 cm⁻¹), and carboxylic acid (1705 and 1250 cm⁻¹) groups was observed via infrared spectroscopy (Figure S1).²² This result is similar to the findings of Cai et al. who observed development of carbonyl and hydroxyl groups in polyethylene after three months of UV exposure in laboratory conditions³ and Brandon et al. who noted formation of hydroxyl and carbonyl groups over time in polyethylene aged in simulated seawater and exposed to sunlight for up to three years.²³

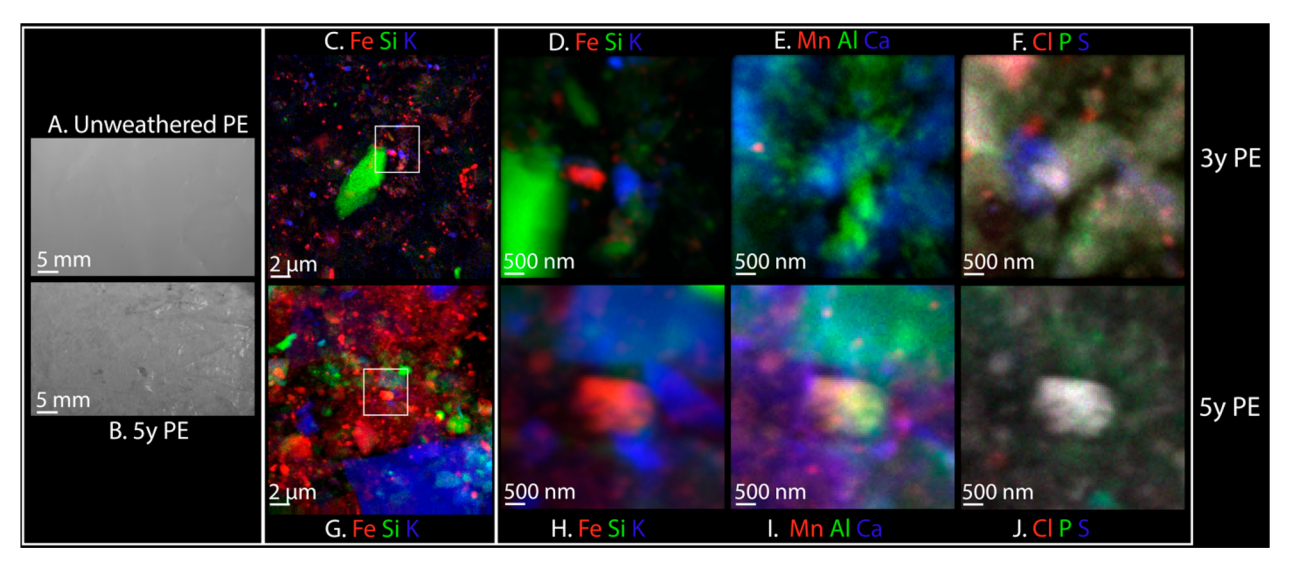


Figure 1. (A, B) Surface of unweathered and five-year weathered PE observed via optical microscopy under 625 nm light. Note the dark particles (B) showing soil inorganics on plastic surface. (C–J) Nanoscale-XRF maps showing elemental distribution in three-year (C–F) and five-year (G-J) terrestrially aged PE. The intensity of RGB (red—green—blue) colors shows relative abundance; white color indicates overlap of the three elements.

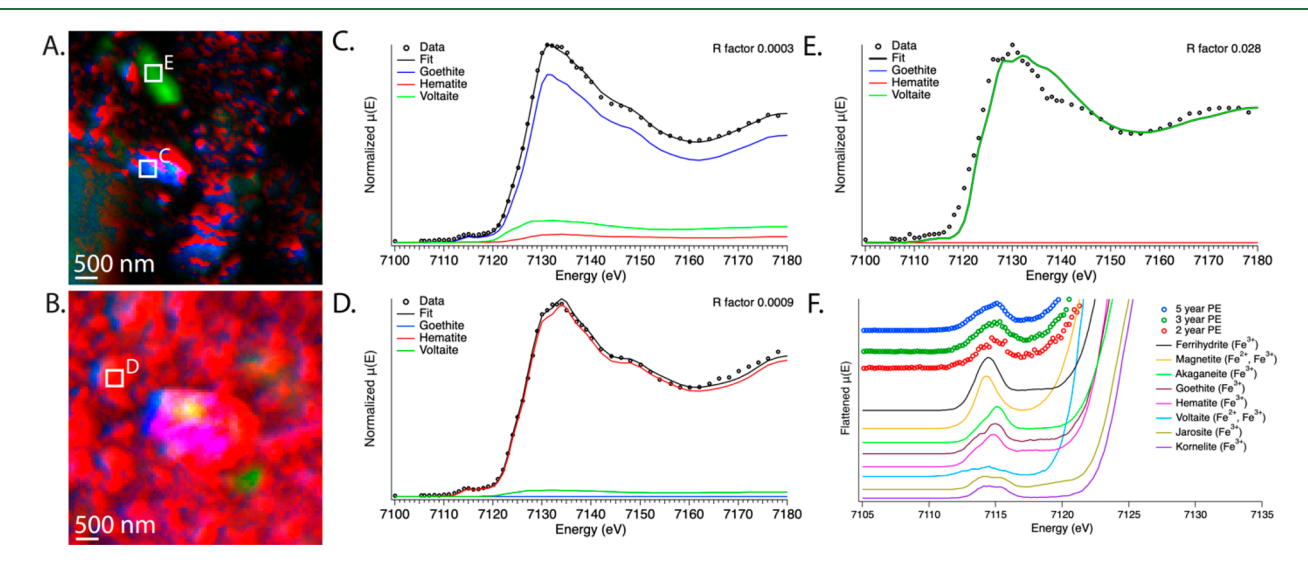


Figure 2. Fe mineral distribution from linear combination fitting (LCF) of Fe K-edge nano-XANES for three-year (A) and five-year (B) weathered PE. In both maps, blue indicates the presence of Fe(III) oxyhydroxides (fit with goethite), red hematite, and green Fe(II)-containing minerals (fit as voltaite). The intensity of color shows the relative abundance of minerals derived by LCF fit. (C-E) Regions of interest that contain areas of abundance for each mineral standard used in the LCF fits. The relative abundance of standards found by LCF fit are indicated by the peak height under the data and fit (black). (F) Comparison of Fe K-edge HERFD-XANES pre-edge region of 2-5-year weathered PE and mineral standards.

Analysis via nano-XRF and scanning electron microscopy found the presence of elements common to soil environments on the surface of plastics (iron (Fe), aluminum (Al), silicon (Si), manganese (Mn), calcium (Ca), potassium (K), chlorine (Cl), phosphorus (P), and sulfur (S)) (Figure 1). The five-year sample was, on average, more enriched than the 3-year sample in Fe (\sim 170 vs \sim 16.7 μ g/cm²), Mn (\sim 3.0 vs \sim 0.40 μ g/cm²), K ($\sim 15.2 \text{ vs } \sim 1.4 \ \mu\text{g/cm}^2$), and Al ($\sim 9.7 \text{ vs } \sim 7.2 \ \mu\text{g/cm}^2$) (error ranges are tabulated in Table S1). As the five-year PE was more oxidized than the three-year PE, the enrichment in Fe and Mn could be due to enhanced electrostatic attraction of these cations by the more aged and oxidized plastic, but could also in part (particularly for Mn) be due to the five-year PE becoming buried in leaf mulch which is known to be enriched in Mn (~800-1300 ppm Fe and ~100-150 ppm Mn at this location). Less, and more amorphous appearing, Ca was

present in the five-year PE (\sim 10.1 μ g/cm²) than the three-year PE (\sim 280 μ g/cm²) (Figure 1, Table S1); this could be due to a more acidic environment within the leaf layer (\sim 4–4.5) than in soil porewater (\sim 7.0–7.6).

Further analyses, including XANES and correlation plots of XRF maps, were used to identify the potential mineral phases of the elements observed. The high correlation between Al and Si indicates the predominance of aluminosilicates, with some observed regions only rich in Si, likely as silicates (Figure S3). The presence of aluminosilicates such as Fe-rich kaolinite and/or smectite was further corroborated by Al–OH–Al (3720–3600 cm⁻¹, 1120–1000 cm⁻¹) and Fe–OH–Al (875 cm⁻¹) bands observed via infrared spectroscopy^{24,25} (Figure S1). The presence of aluminosilicates on weathered plastics is of interest as they could play a role as sorption sites for inorganic contaminants.^{26,27}

The predominant calcium mineral was found via Ca K-edge XANES to be calcite for the 2-year and 3-year PE and a possible disordered humic—calcium complex for the 5-year PE, ²⁸ potentially suggesting more acidic conditions for the five-year sample. Phosphorus and sulfur were highly correlated with calcium in both samples. Due to the significantly higher abundance of Ca relative to P and S, these elements were likely to present as adsorbed species on calcium-rich minerals, e.g., calcite, rather than as apatite or gypsum, particularly for the 3y PE. Bulk Mn K-edge XANES found that Mn was present mainly as Mn (II), suggesting that at times conditions were anoxic on the plastic surface in order to stabilize this phase (Figure S5).^{29,30} Manganese(II) could be further stabilized via adsorption or substitution into carbonates or other mineral phases.³⁰

Ferric and ferrous iron species were observed in all three aged samples via nano- and HERFD-XANES (Figure 2). Ferric species of iron observed to be present via nano-XANES were likely oxides and/or oxyhydroxides commonly found in soils such as hematite, goethite, ferrihydrite, and akageneite. However, further analysis via for example micro- or nano-Xray diffraction is needed to confirm these tentative phase identifications. HERFD-XANES, and in particular pre-edge analysis via HERFD-XANES, was utilized to offer additional insight into phase type and speciation as spectral similarities between Fe(III) (hydr)oxides can be difficult to differentiate using traditional and nano-XANES (Figure S4E).²⁶ Pre-edge peak position and intensity of the samples analyzed via HERFD-XANES were most similar to hematite, akageneite, and goethite (Figure 2F).31 Analysis via HERFD-XANES of the main edge also indicated the presence of ferrihydrite (Figure S4). Thus, there was good agreement between nano-XANES and HERFD-XANES for predominant ferric speciation. The relative abundance of ferrihydrite appeared to decrease with increasing sample age, suggesting the conversion of this metastable phase into perhaps hematite or goethite.²⁶ The presence of Fe(III) (hydr)oxides is of interest as their occurrence is likely to increase sorption capacity toward inorganic contaminants.²⁷ Ferrous iron-containing minerals were also observed via both nano-XANES and HERFD-XANES. These minerals shared some spectral features with magnetite and voltaite; however, these are tentative phase identifications that require diffraction data for further clarification. The bulk abundance of Fe(II)-containing minerals increased with sample age. The presence of ferrous minerals suggests that conditions are at times anoxic on the plastic surface²⁶ and highlights the potential role of Fenton-like reactions in chemical oxidation of the plastic surface.³² Multiple segments were analyzed of the large weathered plastic sheets (approximately 3 m \times 3 m), and relatively homogeneous iron speciation was observed across this large area, suggesting that insights gained via nanoscale-analysis can be applied across larger spatial scales.

Examination of the surface of terrestrially weathered PE via X-ray spectroscopy and microscopy confirms the presence of numerous soil inorganics complexed to aged plastics that have implications for both the mechanisms of plastic degradation and the ability of plastics to complex inorganic contaminants. It is expected that the development of oxygen functional groups on the weathered plastics significantly increases the complexation ability of the plastics toward inorganics including cationic contaminants such as mercury and lead. The presence of ferrous iron has potential significance for the

chemical degradation of plastics as a catalyst in radical-mediated reactions such as Fenton-like reactions. The complexation of inorganic coatings to plastics also has important implications for the sorption of toxic inorganics. Ferrous oxides/oxyhydroxides and aluminosilicates could play key roles in inorganic contaminant sorption to plastics, particularly toxic oxyanions. While this work focused on polyethylene, similar oxidation reactions have been observed on other commonly used plastics. The enrichment of plastics with inorganics warrants further consideration from the perspective of recycling/upcycling as well^{34,35} in order to minimize potential human exposure to toxic metals via leaching from reused plastics. The enrichment of plastics with inorganics warrants further consideration from the perspective of recycling/upcycling as well^{34,35} in order to minimize potential human exposure to toxic metals via

ASSOCIATED CONTENT

Solution Supporting Information

The Supporting Information is available free of charge at https://pubs.acs.org/doi/10.1021/acs.estlett.3c00241.

Method descriptions for XRF, optical microscopy, FTIR, bulk XANES, FTIR spectra, XRF spectra, XRF elemental correlation plots, and XRF elemental counts per square area, Fe K α HERFD-XANES spectra, Mn K-edge bulk XANES spectra, and Ca K-edge bulk XANES spectra (PDF)

AUTHOR INFORMATION

Corresponding Author

Lauren N. Pincus — Department of Geosciences, Princeton University, Princeton, New Jersey 08544, United States; orcid.org/0000-0002-3688-6400; Email: Lpincus@princeton.edu

Authors

Ajith Pattammattel — National Synchrotron Light Source II, Brookhaven National Laboratory, Upton, New York 11973, United States; orcid.org/0000-0002-5956-7808

Denis Leshchev — National Synchrotron Light Source II, Brookhaven National Laboratory, Upton, New York 11973, United States; occid.org/0000-0002-8049-3671

Kewei Zhao – Department of Geosciences, Princeton University, Princeton, New Jersey 08544, United States

Eli Stavitski – National Synchrotron Light Source II, Brookhaven National Laboratory, Upton, New York 11973, United States

Yong S. Chu — National Synchrotron Light Source II, Brookhaven National Laboratory, Upton, New York 11973, United States

Satish C. B. Myneni – Department of Geosciences, Princeton University, Princeton, New Jersey 08544, United States

Complete contact information is available at: https://pubs.acs.org/10.1021/acs.estlett.3c00241

Notes

The authors declare no competing financial interest.

ACKNOWLEDGMENTS

This work was supported by the National Science Foundation under award EAR-PF: 2052956, the Harry H. Hess Postdoctoral Fellowship, the Princeton University Geoscience Department, and the Tuttle and Scott Funds. We thank Ryan Manzuk for his help with microscopy analysis. This research used the HXN, ISS, and TES beamlines of the National

Synchrotron Light Source II, a U.S. Department of Energy (DOE) Office of Science User Facility operated for the DOE Office of Science by Brookhaven National Laboratory under Contract No. DE-SC0012704.

REFERENCES

- (1) Alimi, O. S.; Farner Budarz, J.; Hernandez, L. M.; Tufenkji, N. Microplastics and Nanoplastics in Aquatic Environments: Aggregation, Deposition, and Enhanced Contaminant Transport. *Environ. Sci. Technol.* **2018**, *52* (4), 1704–1724.
- (2) Andrady, A. L. The Plastic in Microplastics: A Review. Mar. Pollut. Bull. 2017, 119 (1), 12–22.
- (3) Cai, L.; Wang, J.; Peng, J.; Wu, Z.; Tan, X. Observation of the Degradation of Three Types of Plastic Pellets Exposed to UV Irradiation in Three Different Environments. *Science of The Total Environment* **2018**, 628–629, 740–747.
- (4) Ashton, K.; Holmes, L.; Turner, A. Association of Metals with Plastic Production Pellets in the Marine Environment. *Mar. Pollut. Bull.* **2010**, *60* (11), 2050–2055.
- (5) Guo, X.; Wang, J. The Chemical Behaviors of Microplastics in Marine Environment: A Review. *Mar. Pollut. Bull.* **2019**, *142*, 1–14.
- (6) Holmes, L. A.; Turner, A.; Thompson, R. C. Adsorption of Trace Metals to Plastic Resin Pellets in the Marine Environment. *Environ. Pollut.* **2012**, *160*, 42–48.
- (7) Holmes, L. A.; Turner, A.; Thompson, R. C. Interactions between Trace Metals and Plastic Production Pellets under Estuarine Conditions. *Marine Chemistry* **2014**, *167*, 25–32.
- (8) Li, M.; He, L.; Zhang, M.; Liu, X.; Tong, M.; Kim, H. Cotransport and Deposition of Iron Oxides with Different-Sized Plastic Particles in Saturated Quartz Sand. *Environ. Sci. Technol.* **2019**, 53 (7), 3547–3557.
- (9) Turner, A.; Holmes, L. A. Adsorption of Trace Metals by Microplastic Pellets in Fresh Water. *Environmental Chemistry* (14482517) **2015**, 12 (5), 600–610.
- (10) Sengupta, M.; Xie, Y.; Lopez, A.; Habte, A.; Maclaurin, G.; Shelby, J. The National Solar Radiation Data Base (NSRDB. Renewable and Sustainable Energy Reviews 2018, 89, 51–60.
- (11) Web Soil Survey; Soil Survey Staff. Natural Resources Conservation Service, United States Department of Agriculture. https://websoilsurvey.nrcs.usda.gov/ (accessed 2/27/2023).
- (12) Soil Survey Geographic (SSURGO) Database for Princeton, NJ. Soil Survey Staff. Natural Resources Conservation Service, United States Department of Agriculture. https://websoilsurvey.nrcs.usda.gov/ (accessed 2/27/2023).
- (13) Thomas, G. W. Soil PH and Soil Acidity. In *Methods of Soil Analysis, Part 3-Chemical Methods*; Sparks, D. L., Page, A. L., Helmke, P. A., Loeppert, R. H., Soltanpour, P. N., Tabatabai, M. A., Johnston, C. T., Sumner, M. E., Eds.; Soil Science Society of America: Madison, Wisconsin, USA, 1996; pp 475–490.
- (14) Pattammattel, A.; Tappero, R.; Ge, M.; Chu, Y. S.; Huang, X.; Gao, Y.; Yan, H. High-Sensitivity Nanoscale Chemical Imaging with Hard x-Ray Nano-XANES. *Sci. Adv.* **2020**, *6* (37), eabb3615.
- (15) Yan, H.; Bouet, N.; Zhou, J.; Huang, X.; Nazaretski, E.; Xu, W.; Cocco, A. P.; Chiu, W. K. S.; Brinkman, K. S.; Chu, Y. S. Multimodal Hard X-Ray Imaging with Resolution Approaching 10 Nm for Studies in Material Science. *Nano Futures* **2018**, 2 (1), 011001.
- (16) Nazaretski, E.; Lauer, K.; Yan, H.; Bouet, N.; Zhou, J.; Conley, R.; Huang, X.; Xu, W.; Lu, M.; Gofron, K.; Kalbfleisch, S.; Wagner, U.; Rau, C.; Chu, Y. S. Pushing the Limits: An Instrument for Hard X-Ray Imaging below 20 Nm. *J. Synchrotron Rad* **2015**, 22 (2), 336–341.
- (17) Yan, H.; Xu, W.; Yu, D.; Heroux, A.; Lee, W.-K.; Li, L.; Campbell, S.; Chu, Y. PyXRF: Python-Based X-Ray Fluorescence Analysis Package. In *X-Ray Nanoimaging: Instruments and Methods III*; Lai, B., Somogyi, A., Eds.; SPIE: San Diego, United States, 2017; p 30. DOI: 10.1117/12.2272585.
- (18) Schindelin, J.; Arganda-Carreras, I.; Frise, E.; Kaynig, V.; Longair, M.; Pietzsch, T.; Preibisch, S.; Rueden, C.; Saalfeld, S.;

- Schmid, B.; Tinevez, J.-Y.; White, D. J.; Hartenstein, V.; Eliceiri, K.; Tomancak, P.; Cardona, A. Fiji: An Open-Source Platform for Biological-Image Analysis. *Nat. Methods* **2012**, *9* (7), 676–682.
- (19) Pattammattel, A.; Tappero, R.; Chu, Y. S.; Ge, M.; Gavrilov, D.; Huang, X.; Yan, H. Hard X-Ray Nano-XANES and Implementation Deep Learning Tools for Multi-Modal Chemical Imaging. In *X-Ray Nanoimaging: Instruments and Methods V*; International Society for Optics and Photonics, 2021; Vol. 11839, p 118390J. DOI: 10.1117/12.2599526.
- (20) Leshchev, D.; Rakitin, M.; Luvizotto, B.; Kadyrov, R.; Ravel, B.; Attenkofer, K.; Stavitski, E. The Inner Shell Spectroscopy Beamline at NSLS-II: A Facility for in Situ and Operando X-Ray Absorption Spectroscopy for Materials Research. *J. Synch. Rad.* **2022**, *29*, 1095—1105.
- (21) Newville, M. Larch: An Analysis Package for XAFS and Related Spectroscopies. J. Phys.: Conf. Ser. 2013, 430, 012007.
- (22) Pavia, D. L.; Lampman, G. M.; Kriz, G. S.; Vyvyan, J. A. *Introduction to Spectroscopy,* 5th ed..; Cengage Learning: Stamford, CT, 2014.
- (23) Brandon, J.; Goldstein, M.; Ohman, M. D. Long-Term Aging and Degradation of Microplastic Particles: Comparing in Situ Oceanic and Experimental Weathering Patterns. *Mar. Pollut. Bull.* **2016**, *110* (1), 299–308.
- (24) Ryan, P. C.; Huertas, F. J. The Temporal Evolution of Pedogenic Fe-Smectite to Fe-Kaolin via Interstratified Kaolin-Smectite in a Moist Tropical Soil Chronosequence. *Geoderma* **2009**, 151 (1-2), 1-15.
- (25) Pincus, L. N.; Ryan, P. C.; Huertas, F. J.; Alvarado, G. E. The Influence of Soil Age and Regional Climate on Clay Mineralogy and Cation Exchange Capacity of Moist Tropical Soils: A Case Study from Late Quaternary Chronosequences in Costa Rica. *Geoderma* **2017**, 308, 130–148.
- (26) Sposito, G. The Chemistry of Soils; Oxford University Press, USA, 2008.
- (27) Violante, A.; Pigna, M. Competitive Sorption of Arsenate and Phosphate on Different Clay Minerals and Soils. *Soil Science Society of America Journal* **2002**, *66* (6), 1788–1796.
- (28) Prietzel, J.; Klysubun, W.; Hurtarte, L. C. C. The Fate of Calcium in Temperate Forest Soils: A Ca K-Edge XANES Study. *Biogeochemistry* **2021**, *152* (2), 195–222.
- (29) Peters, V.; Conrad, R. Sequential Reduction Processes and Initiation of CH4 Production upon Flooding of Oxic Upland Soils. *Soil Biology and Biochemistry* **1996**, 28 (3), 371–382.
- (30) McBride, M. B. Environmental Chemistry of Soils; Oxford University Press: New York, 1994.
- (31) Prietzel, J.; Thieme, J.; Eusterhues, K.; Eichert, D. Iron Speciation in Soils and Soil Aggregates by Synchrotron-Based X-Ray Microspectroscopy (XANES,µ-XANES). European Journal of Soil Science 2007, 58 (5), 1027–1041.
- (32) Lang, M.; Yu, X.; Liu, J.; Xia, T.; Wang, T.; Jia, H.; Guo, X. Fenton Aging Significantly Affects the Heavy Metal Adsorption Capacity of Polystyrene Microplastics. *Science of The Total Environment* **2020**, 722, 137762.
- (33) Mohan, D.; Pittman, C. U. Arsenic Removal from Water/Wastewater Using Adsorbents—A Critical Review. *Journal of Hazardous Materials* **2007**, *1*42 (1), 1–53.
- (34) Mao, S.; Gu, W.; Bai, J.; Dong, B.; Huang, Q.; Zhao, J.; Zhuang, X.; Zhang, C.; Yuan, W.; Wang, J. Migration of Heavy Metal in Electronic Waste Plastics during Simulated Recycling on a Laboratory Scale. *Chemosphere* **2020**, *245*, 125645.
- (35) Turner, A.; Filella, M. Lead in Plastics Recycling of Legacy Material and Appropriateness of Current Regulations. *Journal of Hazardous Materials* **2021**, *404*, 124131.
- (36) Cheng, X.; Shi, H.; Adams, C. D.; Ma, Y. Assessment of Metal Contaminations Leaching out from Recycling Plastic Bottles upon Treatments. *Environmental Science and Pollution Research International* **2010**, 17 (7), 1323–1330.